Catalog No. L51861


# Line Rupture and the Spacing of Parallel Lines

**Contract PR-3-9604**

**Prepared for the**

**Materials Supervisory Committee**

**of**
**Pipeline Research Council International, Inc.**

**Prepared by the following Research Agencies:**

**Battelle Memorial Institute**

**Authors:**
**B. N. Leis**
**S. M. Pimputkar**
**N. D. Ghadiali**

**Publication Date:**
**April 2, 2002**

Pipeline Research Council International Catalog No. L51861



PRCI Reports are Published by **Technical Toolboxes, Inc.**


3801 Kirby Drive, Suite 340
Houston, Texas 77098
Tel: 713-630-0505
Fax: 713-630-0560
Email: info@ttoolboxes.com

## Table of Contents



## List of Tables

## List of Figures

## Pipeline Research Council International, Inc.

P. M. Sørensen, Dansk Olie og Naturgas A/S (Chairman)
J. P. Lucido, ANR Pipeline Company (Vice Chairman)

K. Chano, Osaka Gas Company, Ltd.
R. B. Dun, Transmission Pipelines Australia Pty Ltd.
J. R. Ellwood, Foothills Pipe Lines Ltd.
E. Herløe, Statoil
M. C. Hocking, PG&E Gas Transmission Northwest
R. J. Hummel, Shell E&P Technology Company
D. L. Johnson, Enron Corp
W. A. Johnson, II, El Paso Energy Corporation
G. E. H. Joosten, N. V. Nederlandse Gasunie
R. E. Keyser, CMS Energy
R. B. Maas, Westcoast Energy Inc.
Manager, Consulting Services Dept., Saudi Aramco
S. V. Nanney, Duke Energy Corporation
D. Noble, ARCO Exploration and Production Technology
S. Ricketts, TransCanada PipeLines, Ltd.
N. Rodda, BP Exploration
P. Sandham, TransGas Ltd.
G. Schuler, Columbia Gas Transmission Corp.
N. Schultz, Williams Gas Pipelines - Transco
B. C. Sosinski, Consumers Energy Company
T. M. Steinbauer, Gas Research Institute
G. E. Strang, Southern California Gas Company
M. Tallantyre, BG plc
E. E. Thomas, Southern Natural Gas Company
J. Vainikka, GASUM Oy
G. A. Vaughn, Exxon Production Research Company
M. L. Yoho, CNG Transmission Corp.
G. W. Tenley, Jr. PRC International Staff
A. G. Cotterman, PRC International Staff
B. Dutton, PRC International Staff

## Materials Supervisory Committee

Chairman
H. M. Crump, Enron Corp
Members

W. E. Amend, Southern California Gas Company
M. Anderson, Great Lakes Gas Transmission Company
A. D. Batte, BG Technology
J. Beattie, Foothills Pipe Lines Ltd.
C. Bonar, Transmission Pipelines Australia Pty Ltd.
R. R. Bryant, Union Gas Limited
E. B. Clark, Columbia Gas Transmission Corp.
J. R. Coke, ARCO Exploration and Production
S. P. Cox, Saudi Aramco
B. S. Delanty, TransCanada PipeLines, Ltd.
W. J. DeVries, Consumers Energy Co.
R. E. Graham, TransGas Ltd.
H. H. Haines, Gas Research Institute
C. Juhl, Dansk Olie og Naturgas A/S
A. Korpela, Gasum Oy
V. B. Lawson, Westcoast Energy Inc.
A. C. Madsen, BP Exploration (Alaska) Inc.
B. D. Metzger, El Paso Natural Gas Company
A. Nøklebye, Statoil
T. R. Odom, Williams Gas Pipeline - Texas Gas
Y. Okajima, Osaka Gas Company, Ltd.
G. G. Perkins, Shell Deepwater Development Systems, Inc.
C. W. Petersen, Exxon Production Research Co.
S. Rapp, Duke Energy
A. B. Rothwell, TransCanada PipeLines, Ltd.
P. E. Ruppert, CNG Transmission Corporation
R. W. Scrivner, Williams Gas Pipeline – Transco
W. J. Sisak, Exxon Production Research Co.
W. Sloterdijk, N. V. Nederlandse Gasunie
G. L. Smith, ANR Pipeline Company
P. Stark, Enron Gas Pipeline Group
R. Sutherby, TransCanada PipeLines, Ltd.
G. Vervake, Tennessee Gas Pipeline Company
C. J. Zamarin, Panhandle Eastern Pipeline Co.
G. W. Tenley, Jr., PRC International Staff

**Special thanks to the following PR-3-9604 Ad Hoc Group Members:**

T. R. Odom, Williams Gas Pipeline - Texas Gas (Chairman)
E. B. Clark, Columbia Gas Transmission Company
W. J. DeVries, Consumers Energy Company
R. W. Gailing, Southern California Gas Company
B. D. Metzger, El Paso Natural Gas Company
G. L. Smith, ANR Pipeline Company

# List of Symbols

| | |
|---|---|
| T | Temperature |
| t | Time |
| W | Crater width after rupture is complete (see Figure 1) |
| W(t) | Time-dependent width of crater (parallel to pipe axis) at time, t (see Figure 2) |
| D | Crater depth after rupture is complete (see Figure 1) |
| D(t) | Time-dependent depth of crater at time, t (see Figure 2) |
| $\alpha_1, \alpha_2$ | Respectively, crater wall angle at ground level and at crater half-depth (see Figure 1) |
| a, b | Respectively, the lengths of the semi-minor and semi-major axes of the elliptically shaped crater, see Figure 1 |
| $D_c$ | Depth of cover from ground surface to the center of the pipe (see Figure 1) |
| $D_p$ | Pipe diameter |
| $p_0$ | Gauge pressure inside pipe before rupture |
| w | Soil parameter that is a function of soil type (see Table 1) |
| R(w) | A function of the soil parameter, w, defined for convenience |
| x, y | Coordinates |
| Q | Volume rate of fluid discharge through a round hole in the pipe |
| D | Diameter of round hole in pipe |
| $v_0$ | Discharge velocity through hole in pipe |
| $v_j$ | Velocity on the centerline of a jet formed by fluid emerging from hole in pipe, at a distance x from the hole |
| C | Discharge coefficient that depends on the size and orientation of the hole |
| I, P | Respectively, the impulse and the power of the jet discharging through the hole |
| $\rho_{soil}$ | Density of the soil |
| g | Acceleration due to gravity |
| L, L(t) | Respectively, length from pipe rupture (see Figure 2), and length at time, t |
| $v_{exp}$ | Permissible expansion velocity of the crater as defined in NEN3651 with a recommended value of 1/7200 m/s |
| $R_w$ | Radius of crater formed during a symmetrical guillotine rupture |

| | |
|---|---|
| u, r | Respectively, distance and radius in cylindrical coordinates |
| e, s | Respectively, internal energy and entropy |
| $c_v$ | Specific heat at constant volume |
| c | Speed of sound in the gas |
| $u_x$, $Q_w$ | Respectively, outburst speed of the explosive gases and energy per unit mass of the explosion |
| $r_k$ | Half-width of the crater perpendicular to the axis of the charge |
| $u_{kr}$ | Critical gas velocity such that at greater velocities, soil is displaced |
| R | Universal gas constant with a value 1545 ft-lbf/lbmol-°R |
| $\gamma$ | Specific heat ratio for natural gas with a value of 1.301 for methane |
| $A^{dyn}$ | Denotes the work needed to disturb a unit volume of mass |
| q" | Rate of radiant heat input per unit area |
| E | Rate of heat radiated by flame |
| F | Angle factor between flame and pipe |
| $\tau$ | Transmissivity of the atmosphere, assumed to be unity |
| $\sigma$ | Stefan-Boltzmann constant |
| $\varepsilon_f$ | Flame emissivity, assumed to be unity |
| $T_f$ | Absolute flame temperature |

# Executive Summary

In order to limit the impact of construction on the environment, there is a desire to reduce the spacing between parallel, high-pressure, gas transmission pipelines. Reduced spacing makes a pipeline potentially more vulnerable to incidents on neighboring pipelines. PRCI commissioned Battelle to assess available, equation-based models in terms of applicability to loss of integrity scenarios. The goal is to assist gas companies in determining the spacing that is a practical balance between safe and reliable operation in the event of a rupture of one of the pipelines, and the need to minimize environmental impact.

If loss of integrity of a pipeline is to cause damage to an adjacent pipeline, a particular sequence of events is required. First, loss of integrity of the initiating pipeline leads to the formation of a crater. Second, the escaping gas is ignited and forms a sustained flame. Third, the flame heats the uncovered, adjacent pipeline. This stresses the adjacent pipeline structure, and may cause damage.

Models are needed to evaluate the two physically distinct phenomena in this scenario. A "crater" model is needed to determine the size of the crater formed by the initial loss of integrity. If the crater does not uncover the adjacent pipeline, then the adjacent pipeline cannot be damaged by radiative heating. Crater models based on the pioneering experimental data of Delft Hydraulics are reviewed. An alternative approach based on theory of chemical explosions is presented. Calculations based on these models are compared with data. A conservative scenario is developed by assuming that the escaping gas is always ignited. The consequent radiative heating is modeled numerically for a range of parameters of interest.

Conclusions, based on the foregoing scenario and models, are:

- Pipeline spacings greater than 25 feet (~8 meters) appear to be reasonable in reducing the potential for damage of adjacent pipelines.
- The effect of radiative flame heating diminishes rapidly as distance from the flame increases.
- Continuing gas flow in the adjacent pipeline greatly reduces the chance of damage.
- The soil response to the escaping gas needs to be better understood to obtain improved crater models. It may be that soil tests specifically designed to measure response to fluid impact are needed rather than classical civil engineering tests.

# Report

# on

# Line Rupture and the Spacing of Parallel Lines

**B. N. Leis, S. M. Pimputkar, and N. D. Ghadiali**

## Introduction

High-pressure gas-transmission pipelines have historically been constructed within quite generous right-of-ways. Single-use corridors with widths on the order of 100 feet (~33 m) were not uncommon. As gas demand increased and the right-of-way availability decreased, multiple-use corridors became the norm. This situation increases the chance that an incident on a gas pipeline could affect adjacent services, or cause an incident on an adjacent pipeline. The use of liberal spacings between pipelines has, thus far, limited such occurrences. However, there is a desire to reduce the distance between parallel pipelines with a view to limiting the impact on the environment along the right-of-way. The work presented here was motivated by concern for possible prescriptive regulatory action, driven by environmental and property rights issues, that could mandate the reduction of spacing between adjacent pipelines. This work deals specifically with adjacent high-pressure gas-transmission pipelines.

This report addresses the need for reliable, validated models to assist gas companies in determining the minimum spacing between adjacent pipelines to help ensure safe and reliable operation in the event of a rupture. The objective is to evaluate the exposure of a pipeline due to the rupture and ignition of the escaping gas of an adjacent pipeline. To eliminate semantic confusion, the line that ruptures will be termed the "first" pipeline, and the rupture is termed the "initial" or "original" rupture. The pipeline which is affected by this rupture is termed the "adjacent" pipeline.

The potential thermal damage to an adjacent pipeline as a consequence of the rupture of a pipeline depends on a sequence of seven physical events or conditions:

- Circumstances of the rupture of the first pipeline,
- Fluid dynamics of the jet of gas issuing from the rupture,
- Response of the surrounding soil to the impact of the jet,
- Possible uncovering of the adjacent line,
- Conditions under which the blowing gas ignites,
- Radiative transfer from the ignited gas to the uncovered adjacent pipeline, and
- Response of the adjacent pipeline to the radiative heat input.

Equivalently, one could ask whether the adjacent pipeline would rupture under internal pressure as a result of being exposed to radiative heating after being uncovered by the rupture of the first pipeline. The uncovering of an adjacent pipeline depends on whether the crater caused by the original pipeline rupture is larger than the spacing between the lines. Therefore, the technical basis for determining the safe spacing between adjacent pipelines requires a model to estimate the size of the crater produced by the initial rupture, and a model to estimate the response of the adjacent, uncovered pipeline to radiation from the ignited gas escaping from the original rupture. These models will be termed the "crater" model and the "radiative" model, respectively. These two models in conjunction will allow users to determine whether the adjacent line will survive the rupture of the first line.

The development and application of such a pair of models are presented here. These models are used to formulate line-spacing guidelines to avoid rupture in an adjacent pipeline. The following sections discuss the crater and radiative models.

# Crater Models

## Literature Review of Crater Models and Data

Craters are formed as a result of pipe rupture, and gas flowing from the ruptured pipeline. Two types of rupture are possible:

- a guillotine rupture, where the pipe fails across its diameter, or
- an axial or nearly axial split.

Guillotine ruptures result from cracking around the circumference without significant axial growth. Axial splits can lead to short ruptures where bulging accompanies the split but axial propagation is limited, leading to a spread slit along the length of the pipeline. Axial splits can originate at the top or bottom of the pipe, or the side of the pipe. Depending on the gas composition, temperature, and pressure, the pipeline diameter and wall thickness, and the line pipe steel properties, splits can grow axially, leading to longer ruptures, which terminate when the split spirals around the pipeline leading to a full-bore rupture. It follows that gas can flow from the ruptured pipeline in one of two possible bounding conditions:

- axial or nearly axially leading impinging jet fires, as occurs for guillotine and full-bore ruptures, or
- normal or nearly normal to the length of the pipeline, as occurs for axial or nearly axial contained splits.

The impinging jet fires from the ends of a guillotine rupture have the greatest lateral effect when the flow is axial and the ends of the rupture are relatively close to one another. Such axially impinging jet fires can result from a guillotine break, or from an axial split that develops into a full-bore rupture. Axial splits have the greatest lateral effect when they lie on the side of the pipeline and remain as slits rather than develop into full-bore ruptures. Thus, shorter ruptures tend to be more severe than longer ruptures as a cause of an incident on an adjacent pipeline.

As it is not possible to know, a priori, what type rupture will occur, in the context of spacing of parallel lines, it is reasonable to consirer both guillotine and side slits as potential "worst cases". For this reason craters formed by both guillotine and side-slit ruptures should be evaluated to determine which is predicted to form the bigger crater for the spacing of a parallel line.

Pioneering small-scale experiments undertaken at the Delft Hydraulics Laboratory are the basis of most of the available crater models. These data and a semi-empirical interpretation are discussed in Reference 1. Subsequently, these data were re-examined, and the formulations were enhanced in References 2 through 4. The culmination of this model development as presented in Reference 4 will be referred to as the Gasunie model. In addition, Reference 5 gives formulas applicable to side slit and guillotine ruptures. The side rupture model is hereafter referred to as the NEN 3651 model. The guillotine rupture formula is not explained and attempts to obtain further documentation of this formula were not successful.

The Gasunie model, the NEN 3651 formulas, and a guillotine rupture model based on chemical explosions are discussed next.

## Gasunie Model

### Model Formulation

The loss of integrity of a high-pressure buried pipeline is a complex event. The dimensions of the consequent crater depend on incident-specific factors such as the mode of failure, circumferential location of failure, and relative flows from, and misalignment of, the two pipe ends in the event of a guillotine rupture. Therefore, in order to have any chance of estimating the crater size, it is necessary to make simplifications and approximations that retain the common characteristics of such events. The assumptions, simplifications, and empirical observations that underlie the development of the model, as discussed in Reference 4, are:

- The data in References 1 and 2 are assumed to be applicable.
- The formulation applies to a guillotine rupture wherein two separate pipe ends exist after the rupture.
- The crater is formed in two stages. In the first stage, the pipeline rupture blows out adjacent soil to form a crater whose cross-sectional dimensions including width and depth do not change thereafter. In the second stage, the axially-directed blowing gas jet(s) scour the soil to extend the length of the crater axially.
- The crater cross-sectional shape is assumed to be elliptical as shown in Figure 1. This is based on a comparison of real incidents (which are observed after both crater formation stages are complete) and pipe-fracture tests (which give indications about the crater after the first stage of formation because of rapid reduction in mass flows after rupture). The cross-section of the crater is then completely defined by the width, W, the depth, D, and the crater wall angle, $\psi_1$, shown in Figure 1. Equivalently, the slope of the crater wall at ground level, $\tan\psi_1$, the slope of the crater wall at half-depth, $\tan\psi_2$, and the depth of the crater define the cross-section of the crater because of the assumed elliptical shape. The parameters a and b in Figure 1 are, respectively, the lengths of the semi-minor and semi-major axes of this assumed elliptical shape.
- The soil (including the water content) is assumed to be homogeneous.
- For small fracture lengths, the crater is assumed to be round with the axial length equal to the width.

### Computational Sequence

The inputs to the model are:

- Pipe diameter, $D_p$,
- Pipe pressure, $p_0$,
- Depth of cover from ground surface to the center of the pipe, $D_c$, and
- Qualitative description of the type of soil surrounding the pipe.

For a top rupture, based on observations, little or no soil is removed from under the pipe, and the

crater depth is given by

$$D = D_p + D_c$$

For a guillotine rupture, the crater depth is also a function of type of soil and moisture content, which are characterized by a parameter, w, listed in Table 1.

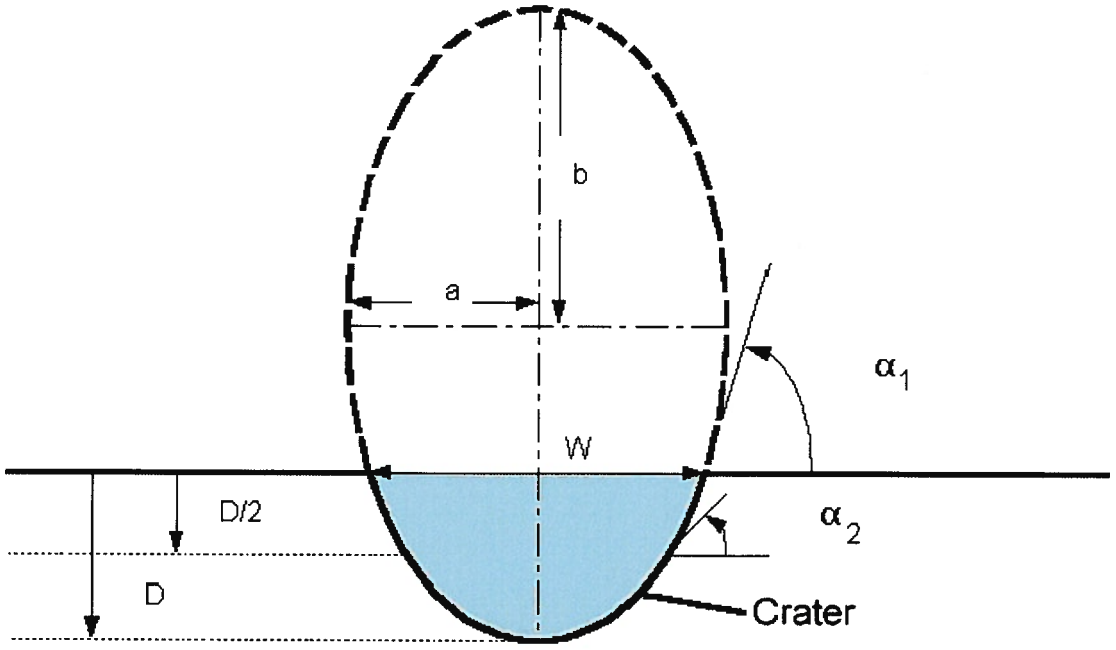


**Figure 1 Representation of crater cross-section as part of an ellipse**

**Table 1 Parameter, w, and crater angles as a function of soil classification**

| Type of Soil | w, dimensionless | $\alpha_1$, degrees | $\alpha_2$, degrees |
|---|---|---|---|
| Very dry sand | 0.75 | 60 | 29 |
| Sand or dry mixed soil | 1.1 | 65 | 35 |
| Mixed soil or gravel | 1.75 | 70 | 45 |
| Humid mixed soil, clay or rock | 2.7 | 75 | 57 |
| Heavy clay | 5 | 80 | 73 |

The depth of the crater, as a function of the soil parameter, w, can be calculated from the following equations, which are from Reference 4 with original attribution to Reference 2. A function of the soil parameter, R(w), is defined for convenience as

$$R(w) = 0.28 + 0.62(5 - w) - 0.07(25 - w^2)$$

for $0.28 < R(w) < 1.3$.

If $w \leq 0.6$

$$D = 4.3D_p + D_c$$

If $0.6 < w < 2$

$$D = \frac{R(w)D_p}{0.3} + D_c$$

If $w \geq 2$

$$D = 2.2D_p + D_c$$

The crater angles are determined from empirical equations that could be improved when additional data become available.

$$\alpha_1 = \tan^{-1}(w+1)$$

$$\alpha_2 = \tan^{-1}\left[\left(\frac{(2.8+0.5w)}{10}\right)(w+1)\right]$$

The formula for $\alpha_2$ is incorrectly missing "arctan" in Reference 4. This was determined by using the sample calculation at the end of Reference 4. Values of the crater angles for some values of w are shown in Table 1.

Knowing the depth D, and the crater angles $\alpha_1$ and $\alpha_2$, the width can be calculated based on the assumption that the shape of the crater is part of an ellipse.

Consider the crater and dimensions shown in Figure 1. The equation of the ellipse is given by

$$\frac{x^2}{a^2} + \frac{y^2}{b^2} = 1$$

Differentiating with respect to x and substituting for x gives

$$\frac{dy}{dx} = -\frac{b}{a}\frac{\sqrt{b^2 - y^2}}{y} \qquad for\, x > 0$$

Evaluating this at the ground level and half crater depth gives

$$\tan\alpha_1 = \frac{b}{a}\sqrt{\left(\frac{b}{b-D}\right)^2 - 1}$$

$$\tan\alpha_2 = \frac{b}{a}\sqrt{\left(\frac{b}{b-0.5D}\right)^2 - 1}$$

These can be solved simultaneously for a and b or a can be eliminated to solve the following equation for b, giving

$$\frac{\sqrt{\left(\frac{b}{b-D}\right)^2 - 1}}{\tan\alpha_1} = \frac{\sqrt{\left(\frac{b}{b-0.5D}\right)^2 - 1}}{\tan\alpha_2}$$

The width of the crater, W, is given by

$$W = 2a\sqrt{1 - \frac{(b-D)^2}{b^2}}$$

The sample calculation in Reference 4 uses the following inputs:

$D_p = 0.75$ m
$D_c = 1.2$ m
$p_0 = 70$ bar
$w = 1.75$

The outputs are:

$D = 3.1$ m
$W = 9.8$ m

A Mathcad® worksheet for this case is provided in Appendix A, along with a printed version.

## NEN 3651 Equations

NEN 3651 lists equations to calculate the dimensions of craters and erosion pits formed by breached pipelines. Two formulations are relevant for leaks and ruptures in high-pressure gas pipelines: that for side leaks, and that for ruptures. The formulas for these cases and their antecedents as far as were determined are discussed next.

**Side-Slit Rupture**

In the late 1960s and early 1970s, Delft Hydraulics Laboratory conducted experimental studies on craters formed by breaks in water and gas pipes (Reference 1). The formulations were revised in 1991 (Reference 3) although no new data were used. The analysis of the data and the formulation of a model used dimensional analysis to obtain the functional form of the parametric relations, which were then calibrated by test data and incident data. A summary is presented next.

The analytical development is based on the following conceptualizations:

- The efflux acts like a three-dimensional jet in a uniform medium,
- The depth of the crater is primarily determined by the depth of burial of the pipe and the local soil conditions, especially the moisture content,
- Once the near-field crater is formed (in the immediate vicinity of the pipe), the crater grows longer and wider but the depth remains unchanged, and
- The growth of the crater in time is a result of the efflux progressively eroding the soil to form a widening crater.

The mathematical arguments emphasize the parametric relationships with the constants being specified by empirical calibration.

Consider a pipeline with a side leak as shown in Figure 2. The crater that is progressively formed by soil erosion has width W and depth D at a distance L from the pipe at time t after the leak occurs. The volume rate of discharge of a fluid, Q, through a round hole of diameter d at a velocity of $v_0$ is given by

$$Q = C \frac{\pi}{4} d^2 v_0$$

where C is the discharge coefficient that depends on the size and orientation of the hole. The impulse, I, and the power of the jet, P, are defined as

$$I = \rho Q v_0$$

$$P = \frac{1}{2} \rho Q v_0^2$$

The velocity on the centerline of a jet at a distance x, $v_j$ is given by

$$v_j = 6 \frac{d}{x} v_0$$

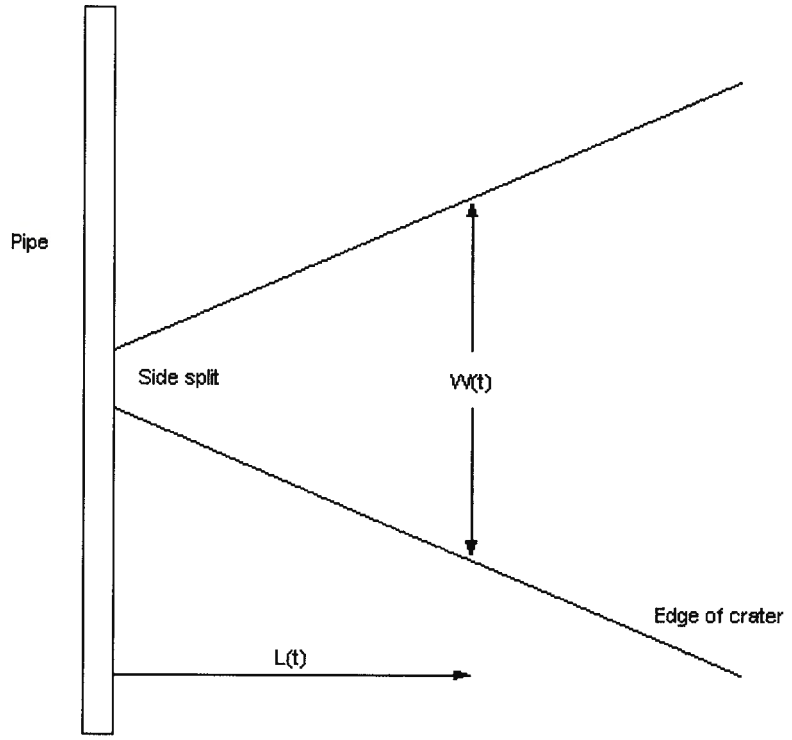


**Figure 2 Schematic of side-slit rupture**

By using Bagnold's theory of stream power (Reference 6), a differential equation for the length of the crater is obtained as

$$\rho_{soil}\, g\, D\, W \frac{dL}{dt} \approx \frac{1}{2} \rho\, v^3\, W,$$

Where $\rho_{soil}$ is the density of the soil, and g is the acceleration due to gravity.

The solution obtained by assuming the power is constant, integrating and imposing the initial condition L = 0 at t = 0, is

$$L = R(w)\left(\frac{g}{D^2}\left(\frac{I}{\rho_{soil} g}\right)^3 t^2\right)^{\frac{1}{8}}$$

The factor R(w) is introduced to account for the fact that the original test data applied only to sandy soils. R(w) is a function of soil cohesion and is to be determined from experimental measurements. It is noted that the above solution defines a crater that increases monotonically with increasing time.

At this stage, the authors of References 1 and 3 suggest that time can be eliminated from

this expression by using a relationship postulated on the basis of dimensional equivalence:

$$\frac{dL}{dt} \approx \sqrt{gL}$$

The equation in NEN 3561 can actually be obtained directly in the following way. Substituting the centerline jet velocity, $v_j$, for the velocity, v, and in turn substituting for $v_0$, we obtain:

$$\rho_{soil}\, g\, D \frac{dL}{dt} \approx \frac{1}{2}\rho\left[\frac{6d}{L}\sqrt{\frac{4I}{\rho C \pi d^2}}\right]^3$$

Solving for L gives:

$$L = \frac{12}{\sqrt{\pi C}}\left(\frac{\rho}{2\rho_{soil}}\right)\frac{1}{\left(gD\frac{dL}{dt}\right)^{\frac{1}{3}}}\left(\frac{I}{\rho}\right)^{\frac{1}{2}}$$

which, after rearranging gives:

$$L = \frac{12}{\sqrt{\pi C}}\left(\frac{\rho}{2\rho_{soil}}\right)\frac{\left(\frac{g}{D^2}\left(\frac{I}{\rho g}\right)^3\right)^{\frac{1}{6}}}{\left(\frac{dL}{dt}\right)^{\frac{1}{3}}}$$

Further, recognizing the order-of-magnitude nature of the development, the leading term can be replaced by an empirical factor that is soil-dependent. Thus introducing the concept of R(w) and using the format and nomenclature of NEN3651 Annex, page 61, one obtains:

$$G_B = \sqrt[3]{\frac{R(w)^4}{4}}\,\frac{\left(\frac{g}{D^2}\left(\frac{I}{\rho g}\right)^3\right)^{\frac{1}{6}}}{\left(v_{exp}\right)^{\frac{1}{3}}}$$

where $G_B$ corresponds to L in the present notation and $v_{exp}$ is the "permissible expansion velocity" of the crater. NEN3561 recommends that "initially" a value of 1/7200 m/s be used for $v_{exp}$. NEN3651 further states that if "$G_B > b_0$", or in the nomenclature used here, L > d, then the width of the crater, W, ($G_L$ in the nomenclature of NEN 3651) is given by:

$$W = \frac{(L+d)}{2}\,.$$

**Guillotine Rupture**

Assuming that the guillotine rupture produces a symetrical crater as occurs for an explosive rupture, NEN 3651 gives the radius of the crater, $R_w$, as:

$$R_w = \sqrt{0.64(D_p^3 p_0)^{\frac{2}{3}} + 0.65 D_c (D_p^3 p_0)^{\frac{1}{3}} - 0.83 D_c^2} \quad .$$

Details of the development of this equation are limited and attempts to obtain further documentation were unsuccessful. As such, it is not possible to provide discussion concerning its development or the underlying assumptions.

## Development of a Crater Model

Craters caused by explosions are of interest in the development of ordnance. Some of the physics are similar to that governing crater formation of a pipeline rupture in that the size of the crater depends on the strength of the explosive, the depth of burial and the characteristics of the surrounding soil. Such a crater formation theory was used to estimate the width of a crater caused by the rupture of a pipeline. The basis of the mathematical formulation is taken from the theory of chemical explosions as outlined in Henrych (Reference 7). For consistency, Henrych's nomenclature has been changed to that used in this report.

To determine whether an adjacent pipeline is uncovered in the course of a rupture, it is adequate to calculate the crater cross-section perpendicular to the axis of the ruptured pipeline. This cross-section is established in the first stage in the two-stage Gasunie model as noted earlier. This view of staged crater formation was also adopted for the ordnance model, and the crater cross-section formation process was assumed to be two-dimensional. The dimensions of the crater cross-section were calculated by modeling the crater as being formed by the explosion of an infinitely long buried charge.

The one-dimensional equations governing gaseous explosions of a cylindrical charge are

$$\frac{\partial \rho}{\partial t} + u\frac{\partial \rho}{\partial r} + \rho\frac{\partial u}{\partial r} + \frac{\rho u}{r} = 0$$

$$\frac{\partial u}{\partial t} + u\frac{\partial u}{\partial r} + \frac{1}{\rho}\frac{\partial p}{\partial r} = 0$$

$$T\frac{ds}{dt} = \frac{de}{dt} - \frac{p}{\rho^2}\frac{d\rho}{dt}$$

$$p = \rho R T$$

$$e = c_V T - \int_{\rho_0}^{\rho} \left[ T\left(\frac{\partial p}{\partial T}\right)_{\rho} - p \right] \frac{d\rho}{\rho^2}$$

supplemented by empirical relationships, as necessary.

For an explosion in an incompressible medium bounded by a free surface, if the energy of the explosion is instantaneously converted into energy of the explosive wave, the outburst speed of the explosive gases, $u_x$, can be expressed as:

$$u_x = \sqrt{\frac{2\rho_0 Q_w}{3\rho_{soil}}}$$

where $Q_w$ is the energy per unit mass of the explosion. If the detonation velocity is taken to be equal to c, the speed of sound at the pressurized gas conditions prior to rupture, $Q_w$ can be expressed as (Reference 7)

$$Q_w = \frac{c^2}{2(\gamma^2 - 1)}$$

where $\gamma$ is the specific heat ratio for natural gas.

The speed of sound is expressed in terms of the gas conditions as

$$c = \sqrt{\gamma R T}$$

The half-width of the crater perpendicular to the axis of the charge, $r_k$, can be shown to be given by

$$r_k = \sqrt{\frac{u_x D_p D_c}{u_{kr}} - D_c^2}$$

where $u_{kr}$ is the critical velocity defining the boundary between the gas velocity that can displace soil and the gas velocity that cannot.

$$u_{kr} = \sqrt{\frac{2A^{dyn}}{\rho}}$$

$A^{dyn}$ denotes the work needed to disturb a unit volume of mass. It depends on the characteristics of the soil surrounding the pipe, and needs to be determined empirically as a function of the classical civil engineering classification of soils. In the absence of such information, $A^{dyn}$ was effectively determined empirically by determining the average value of $u_{kr}$ from a small subset (eight cases) of the 42 cases examined herein. This subset was randomly selected and no attempts were made to optimize the subset or the values obtained for $u_{kr}$. The average value of $u_{kr}$ found from the subset was then used without modification for all the data comparisons.

For an average value of $u_{kr}$ = 0.617 m/s, and a soil density of 2050 kg/m$^3$, the value of $A^{dyn}$ is 390 Pa.

## Validation of the Crater Model Using Data Available at Battelle and Elsewhere

Battelle has been active in pipeline incident investigation for many years. In this time, Battelle has accumulated information on many pipeline ruptures. These data include the operating conditions of the pipeline and the size of the resultant crater. This database has been augmented by information supplied by several gas companies. The complete database contains axial splits as well as guillotine ruptures both for typical pipeline construction and construction through rock trenches. Crater sizes calculated on the basis of the Gasunie and Battelle models were compared with data. These two models are formulated with different approaches: the Gasunie model relies on experiments, while the Battelle model uses the framework derived from the gas dynamics of chemical explosions. The agreement of both models with the data is comparable.

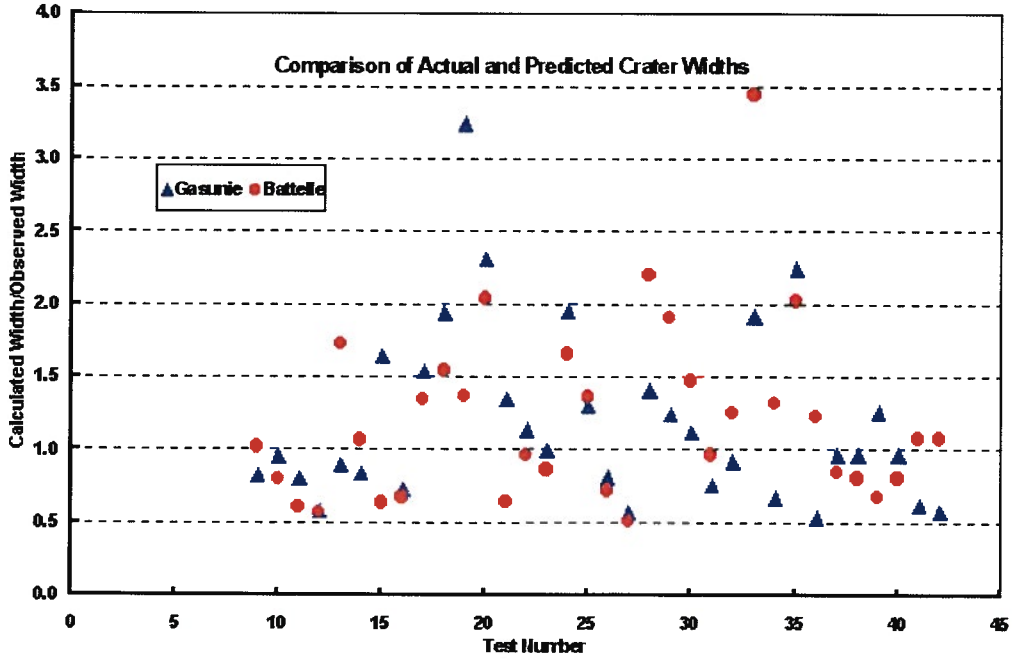


**Figure 3 Comparison of data and model calculations**

This is shown in two ways. First the ratio of the calculated crater width to the measured crater width is plotted for each of the 42 cases for which data are available. This is shown in Figure 3. The x-axis shows the incident number that was sequentially assigned to each test case and has no intrinsic physical significance.

The data were also divided into bins for display as histograms as shown in Figure 4. Again, it is evident that the models are of comparable validity.

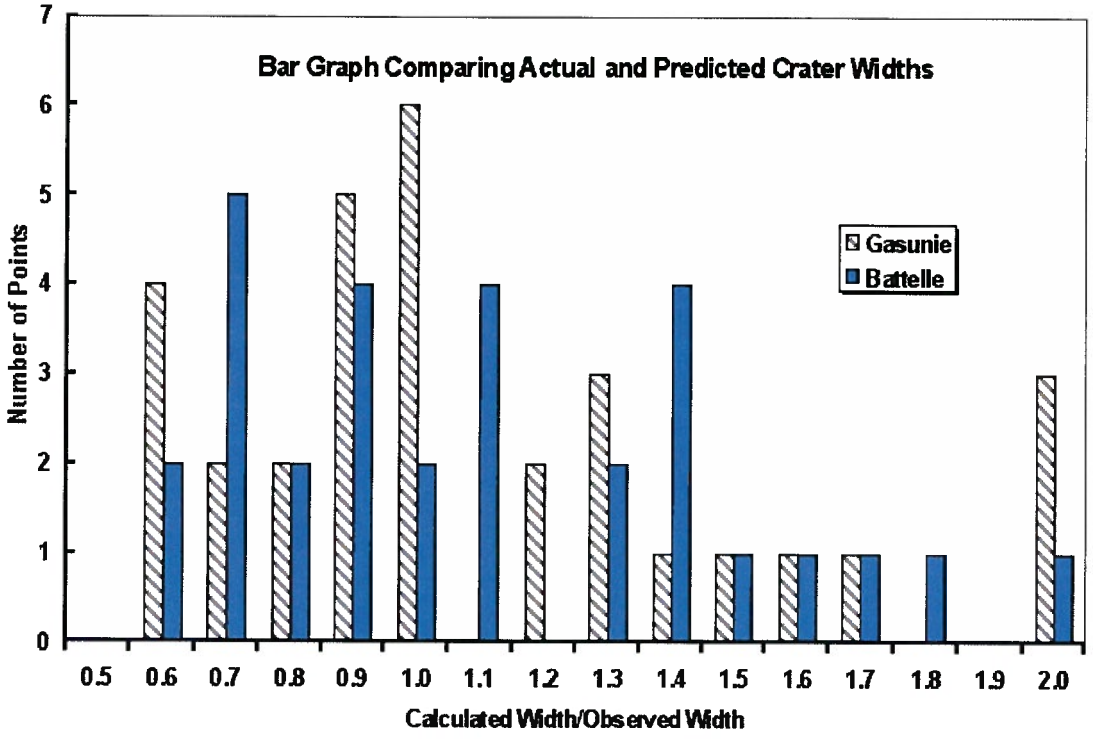


**Figure 4 Histogram comparison of models for 42 cases for which data are available**

## Radiative Model

### Development of a Radiative Damage Model

In developing the radiative damage model, it was assumed that the adjacent pipeline runs parallel to the first pipeline. The adjacent pipeline is partially uncovered when the first pipeline ruptures and forms a crater. This scenario requires that the space between the pipelines is less than the crater width. Blowing gas from the rupture is assumed to be ignited, forming a fiery plume. The plume is approximated as a cone defined by its half angle. Thermal radiation from the plume impacts the uncovered portions of the adjacent pipeline on a line-of-sight basis. Thus, portions of the adjacent pipeline that can "see" the plume are heated by incident thermal radiation. The thermal energy from the radiation is partly conducted radially through the pipe wall, and partly conducted circumferentially around the pipe wall. In either case, the heat is assumed to be carried away by the gas flowing in the adjacent pipeline. The temperature of the flowing gas increases as a consequence. This sequence is shown schematically in Figure 5.

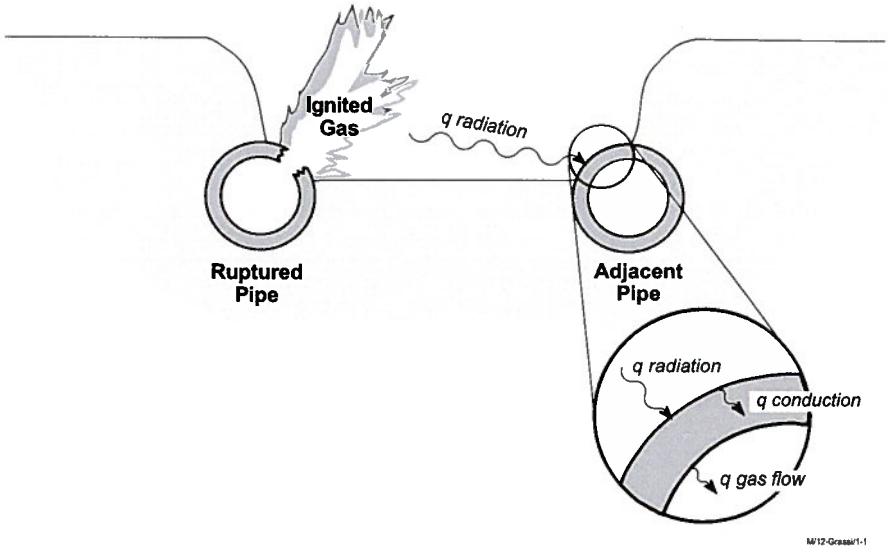


**Figure 5 Schematic representation of heat transfer from gas plume to gas in adjacent pipe**

A commercially available finite-element model, ABAQUS, was used to compute the temperature fields resulting from the foregoing scenario. ABAQUS/Standard is a general-purpose, production-oriented finite-element program designed for analyzing a wide variety of problems. The time- and frequency-domain analysis procedures available in ABAQUS/Standard can be divided into two classes: "general analyses" and "linear perturbation analyses".

The "general analyses" category includes applications in static stress and displacement analysis, viscoelastic and viscoplastic response, transient or steady-state heat transfer, transient

dynamic stress and displacement, and coupled thermal-mechanical analysis. The "linear perturbation analyses" category includes static stress/displacement analysis, and dynamic stress/displacement analysis. Other features of the program are:

- A large number of material models,
- Structural elements including beams, shells, and other solids,
- Modeling of interactions between bodies,
- Prescribed boundary conditions, and
- Special features such as restart of simulations and user-defined subroutines.

Features of ABAQUS/Standard that made it particularly suitable for the current analysis included the ability to:

- Analyze conduction, radiation, and forced convection,
- Model the flame, pipe and the gas with different elements,
- Model the interface between the gas (fluid) and the pipe (structure), and

Use macros to generate mesh with different input parameters such as pipe size, spacing, and gas flow rates.

The finite element model geometry was divided into three regions consisting of the flame, the gas, and the pipe. The complete simulation consisted of 1,683 nodes, 160 flame elements, 160 pipe elements, and 640 gas elements. The 8-node, solid, heat transfer element (designated as the "DC3D8" element in ABAQUS) was selected to represent the three regions in the simulation. The simulations were run until steady state was obtained.

The model is shown in Figure 6. Figure 7 shows an enlarged view of the pipe/gas elements. The mesh was generated using FEMAP (another commercially available computer program) and was then exported to ABAQUS. A macro was written for FEMAP to generate the various parts of the model automatically when the following parameters were provided: plume (flame) half-angle and height, distance between pipelines, and diameter and wall thickness of the adjacent pipe.

The boundary conditions and property data that were used are:

- Flame temperature — 1,200° C,
- Pipe and gas initial temperature — 15° C,
- Emissivity of flame surface — 1.0,
- Emissivity of pipe surface — 0.8, and
- Convective heat transfer from the wall of the adjacent pipe to the flowing gas.

The pipe material properties that were obtained from Reference 1 for a pressure of 1000 psi at 15 C were:

- Conductivity — 50 W/m °C,
- Density — 7,800 kg/m$^3$, and,
- Specific Heat — 500 J/kg °C.

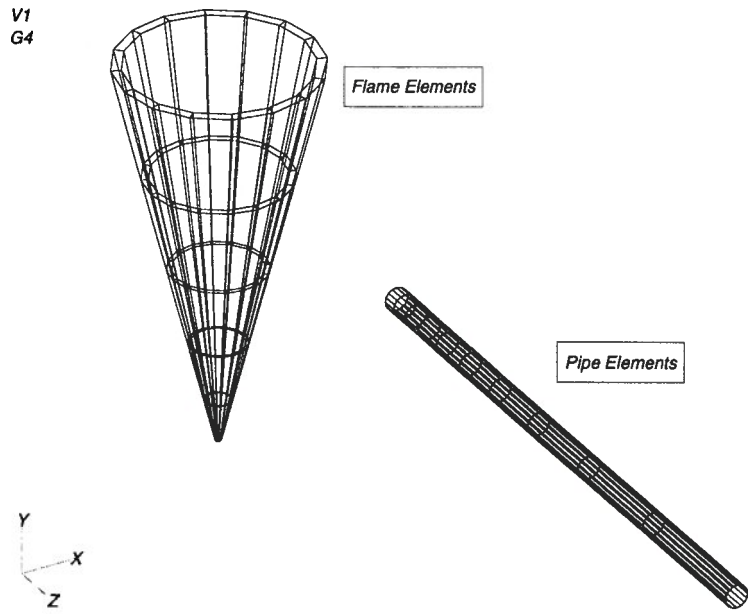


**Figure 6 Overview of finite element model**

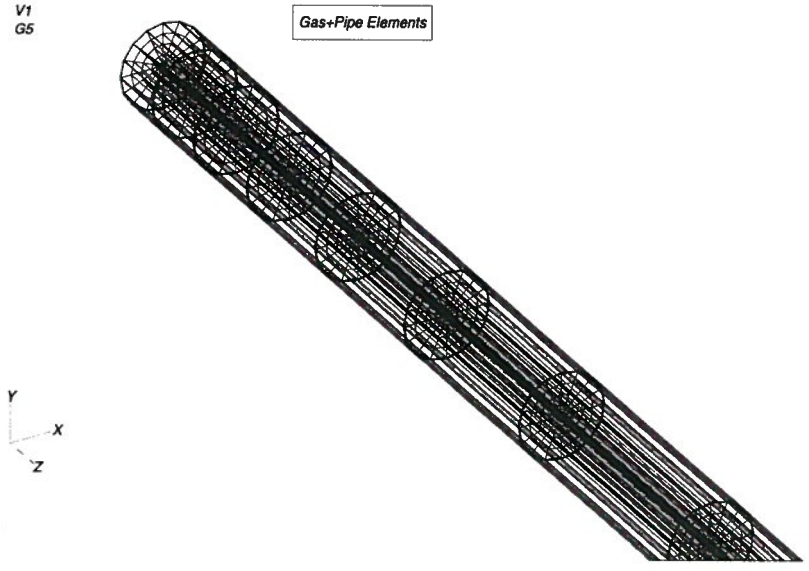


**Figure 7 View of pipe elements**

The range of parameters considered in the analysis were:

- Pipe diameter (0.610, 0.762 and 1.067 meters),
- Pipe wall thickness (6.35, 7.950 and 14.427 mm),
- Length of adjacent pipe (20 meters),
- Gas velocity (5, 10, and 15 miles per hour),
- Flame height (180 meters), and
- Flame cone angle (7, 14, and 27 degrees)

A gas velocity of zero miles-per-hour was not considered because it represents stagnant gas. In a steady state model, with no heat removed by the gas, the flame viewing side of the pipe would receive heat and the other side would have to radiate all the heat. This would cause gradients that would cause the pipe to fail within minutes and the computer simulation to become unstable.

The input parameters that are required for the model are plume half-angle, radiative flame temperature, distance between pipelines, diameter and wall thickness of the adjacent pipeline, and gas flow rate in the adjacent pipeline. The input parameters represent physical variables that are expected to affect pipe spacing. The flame temperature and the flame emissivity determine the amount of heat radiated. The flame height, plume half-angle, and the pipe spacing determine the amount of heat incident on the adjacent pipe. The dimensions of the adjacent pipe and the gas flow velocity determine the temperature distribution in the adjacent pipe. In the computer simulations, these parameters were varied to identify their importance in determining the resultant wall temperature distribution in the adjacent pipe.

The radiative flame temperature was taken to be 1,500 K based on values given in Reference 8. Data from the fireball created in the second Alliance Pipeline Co full-scale test, done at the British Gas test site at Spadeadam UK and overseen on behalf of Alliance by one of the authors, validate the use of this flame temperature as follows. The radiometer data were plotted as a function of distance from the fireball. Theses data are shown as discrete points in Figure 8. The radiometer surfaces were tilted with respect to the horizontal so that they would see the fireball. The fireball was approximated as a vertical cylinder with radius 30 m and height 300 m. These values were selected after visual examination of a photograph of the fireball and were not optimized in any way. The heat received by the radiometer surfaces, q″, is given by

$$q'' = E\, F\, \tau$$

where F is the angle factor between the flame and the tilted element, $\tau$ is the transmissivity of the atmosphere (assumed to be unity), and E is the radiation emitted by the flame and is given by

$$E = \sigma\, \varepsilon_f\, T_f^4$$

where $\sigma$ is the Stefan-Boltzmann constant, $\varepsilon_f$ is the flame emissivity (assumed to be unity), and $T_f$ is the flame temperature.

Using the angle factors given in Reference 9, the radiation received by the radiometers as

a function of distance and angle of tilt was calculated for a flame temperature of 1,500 K. It is shown in Figure 8 as a solid line. The agreement is good. This validates the use of the assumed flame temperature.

Table 2 lists the computer predictions that have been made and the associated input parameters. The following parameters were derived from temperatures computed in the adjacent pipe:

- Maximum temperature,
- Maximum radial temperature gradient,
- Maximum circumferential temperature gradient, and
- Maximum axial temperature gradient.
- The radial temperature gradient is the "through-wall" temperature gradient, the circumferential temperature gradient and the axial gradient are the average gradient in the circumferential and axial direction in the pipe wall.

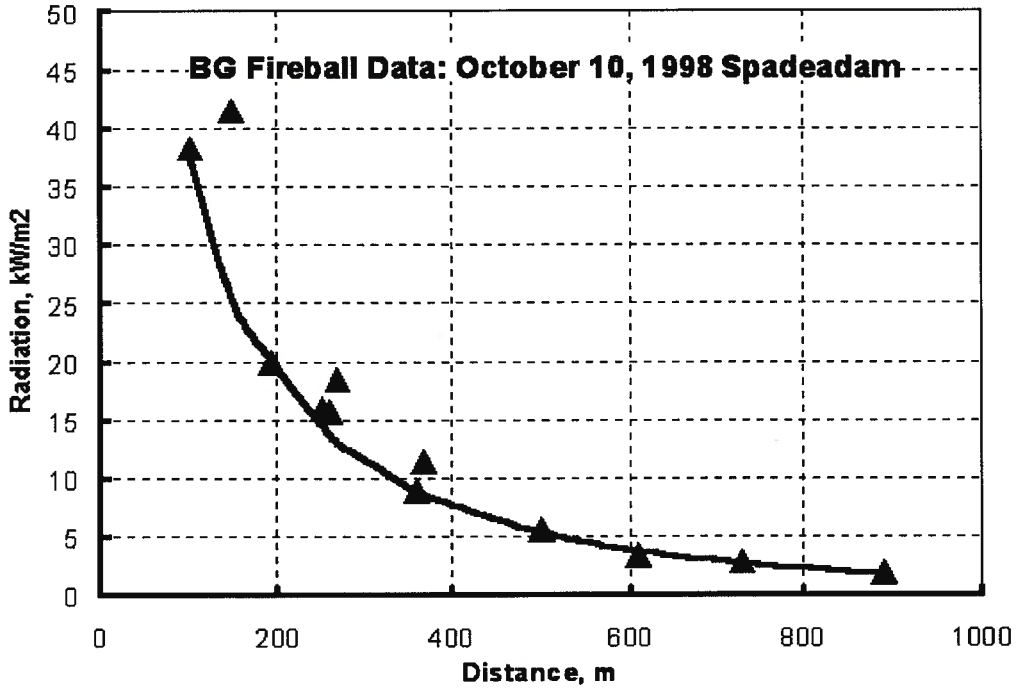


**Figure 8 Comparison of thermal radiation data with calculations**

In the absence of a complete structural analysis of the adjacent pipe, these parameters were judged to provide a good indication of the locations and relative magnitudes of high thermal stress in the adjacent pipeline. Figure 9 shows a typical color-coded output from the finite-element program for the predicted temperature on the exterior of the pipe. Figure 10 shows the predicted temperature for a cross-section through the pipe and the gas.

**Table 2 Input matrix (SI units)**

| Job No. | Name | Flame Half Cone Angle | Spacing, meters | Pipe Diameter, meters | Pipe Wall, meters | Gas Velocity, meters/sec |
|---|---|---|---|---|---|---|
| 1 | Sopl1 | 14 | 7.620 | 0.762 | 0.008 | 0.447 |
| 2 | Sopl2 | 7 | 7.620 | 0.762 | 0.008 | 0.447 |
| 3 | Sopl3 | 27 | 7.620 | 0.762 | 0.008 | 0.447 |
| 4 | Sopl4 | 14 | 7.620 | 0.762 | 0.008 | 2.235 |
| 5 | Sopl5 | 14 | 7.620 | 0.762 | 0.008 | 4.470 |
| 6 | Sopl6 | 14 | 7.620 | 0.762 | 0.008 | 6.706 |
| 7 | Sopl7 | 14 | 7.620 | 0.610 | 0.006 | 2.235 |
| 8 | Sopl8 | 14 | 7.620 | 0.610 | 0.006 | 4.470 |
| 9 | Sopl9 | 14 | 7.620 | 0.610 | 0.006 | 6.706 |
| 10 | Sopl10 | 14 | 7.620 | 1.067 | 0.014 | 2.235 |
| 11 | Sopl11 | 14 | 7.620 | 1.067 | 0.014 | 4.470 |
| 12 | Sopl12 | 14 | 7.620 | 1.067 | 0.014 | 6.706 |
| 13 | Sopl13 | 14 | 3.048 | 0.762 | 0.008 | 0.447 |
| 14 | Sopl14 | 7 | 3.048 | 0.762 | 0.008 | 0.447 |
| 15 | Sopl15 | 27 | 3.048 | 0.762 | 0.008 | 0.447 |
| 16 | Sopl16 | 14 | 3.048 | 0.762 | 0.008 | 2.235 |
| 17 | Sopl17 | 14 | 3.048 | 0.762 | 0.008 | 4.470 |
| 18 | sopl18 | 14 | 3.048 | 0.762 | 0.008 | 6.706 |
| 19 | sopl19 | 14 | 3.048 | 0.610 | 0.006 | 2.235 |
| 20 | sopl20 | 14 | 3.048 | 0.610 | 0.006 | 4.470 |
| 21 | sopl21 | 14 | 3.048 | 0.610 | 0.006 | 6.706 |
| 22 | sopl22 | 14 | 3.048 | 1.067 | 0.014 | 2.235 |
| 23 | sopl23 | 14 | 3.048 | 1.067 | 0.014 | 4.470 |
| 24 | sopl24 | 14 | 3.048 | 1.067 | 0.014 | 6.706 |
| 25 | sopl25 | 14 | 15.240 | 0.762 | 0.008 | 0.447 |
| 26 | sopl26 | 7 | 15.240 | 0.762 | 0.008 | 0.447 |
| 27 | sopl27 | 27 | 15.240 | 0.762 | 0.008 | 0.447 |
| 28 | sopl28 | 14 | 15.240 | 0.762 | 0.008 | 2.235 |
| 29 | sopl29 | 14 | 15.240 | 0.762 | 0.008 | 4.470 |
| 30 | sopl30 | 14 | 15.240 | 0.762 | 0.008 | 6.706 |
| 31 | sopl31 | 14 | 15.240 | 0.610 | 0.006 | 2.235 |
| 32 | sopl32 | 14 | 15.240 | 0.610 | 0.006 | 4.470 |
| 33 | sopl33 | 14 | 15.240 | 0.610 | 0.006 | 6.706 |
| 34 | sopl34 | 14 | 15.240 | 1.067 | 0.014 | 2.235 |
| 35 | sopl35 | 14 | 15.240 | 1.067 | 0.014 | 4.470 |
| 36 | sopl36 | 14 | 15.240 | 1.067 | 0.014 | 6.706 |
| 37 | sopl37 | 14 | 4.572 | 0.762 | 0.008 | 2.235 |
| 38 | sopl38 | 14 | 4.572 | 0.762 | 0.008 | 4.470 |
| 39 | sopl39 | 14 | 4.572 | 0.762 | 0.008 | 6.706 |
| 40 | sopl40 | 14 | 4.572 | 0.610 | 0.006 | 2.235 |
| 41 | sopl41 | 14 | 4.572 | 0.610 | 0.006 | 4.470 |
| 42 | sopl42 | 14 | 4.572 | 0.610 | 0.006 | 6.706 |
| 43 | sopl43 | 14 | 4.572 | 1.067 | 0.014 | 2.235 |
| 44 | sopl44 | 14 | 4.572 | 1.067 | 0.014 | 4.470 |
| 45 | sopl45 | 14 | 4.572 | 1.067 | 0.014 | 6.706 |
| 46 | sopl46 | 14 | 6.096 | 0.762 | 0.008 | 2.235 |
| 47 | sopl47 | 14 | 6.096 | 0.762 | 0.008 | 4.470 |
| 48 | sopl48 | 14 | 6.096 | 0.762 | 0.008 | 6.706 |
| 49 | sopl49 | 14 | 6.096 | 0.610 | 0.006 | 2.235 |
| 50 | sopl50 | 14 | 6.096 | 0.610 | 0.006 | 4.470 |
| 51 | sopl51 | 14 | 6.096 | 0.610 | 0.006 | 6.706 |
| 52 | sopl52 | 14 | 6.096 | 1.067 | 0.014 | 2.235 |
| 53 | sopl53 | 14 | 6.096 | 1.067 | 0.014 | 4.470 |
| 54 | sopl54 | 14 | 6.096 | 1.067 | 0.014 | 6.706 |

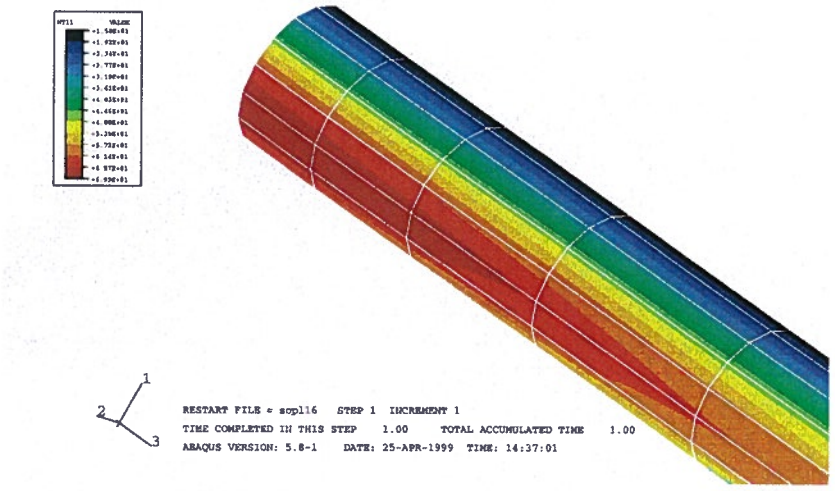


**Figure 9 Typical temperature distribution for pipe outside wall temperature**

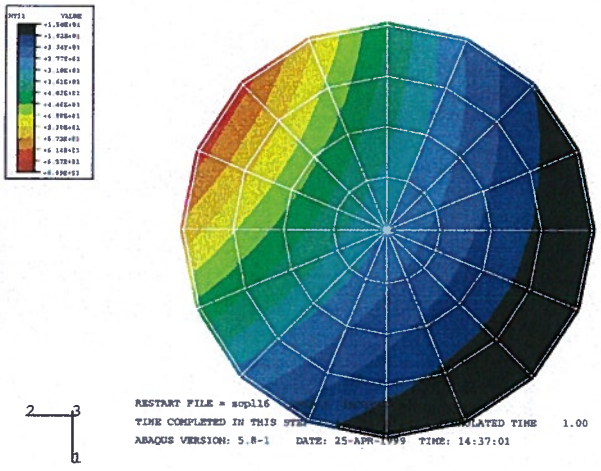


**Figure 10 Typical temperature distribution for cross-section through pipe**

Figures 11 and 12 show views of actual ruptures of different lengths with burning gas. In Figure 11, the flame is quite high in comparison to its width, which is typical of shorter ruptures. In contrast, the view in Figure 12 shows a fire burning over a much longer fracture, which is about ten times the length of that in Figure 11. Although the flame burns over a greater length, its width is on the same order as that shown in Figure 11. Were the fire ball broader than in Figure 11, it could be expected to affect a nearby pipeline more than the narrow flame. This tendency is clearly evident in the numerical results shown in Figure 13, which are predictions for a pair of pipelines spaced at 7.62 m (25 ft). As the flame becomes broader, the most pronounced effect is on the radial gradient. The axial gradient, as is intuitively reasonable, is essentially unaffected.

**Figure 11 View of short rupture**

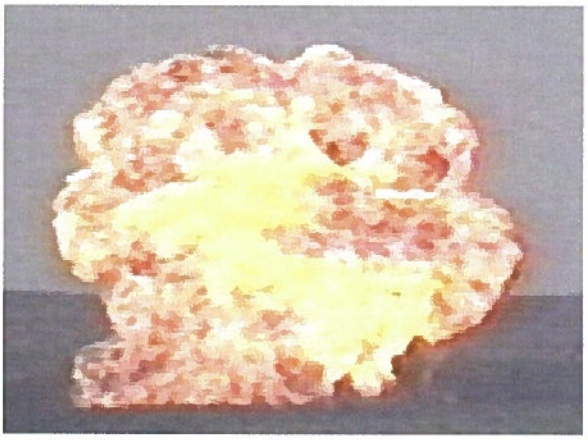

**Figure 12 View of long rupture**

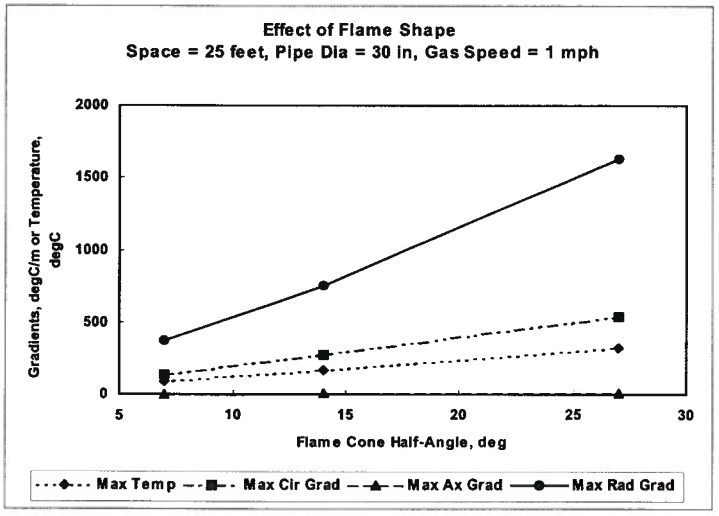


**Figure 13 Computed maximum temperature and temperature gradients in adjacent pipe as a function of flame shape**

Figure 14 shows the effect of gas flow rate (represented by gas speed) with spacing, adjacent pipe diameter and flame shape constant. As the gas flow increases, heat is convected away more quickly and the maximum temperature and the circumferential temperature gradient diminish rapidly. The axial temperature gradient is negligible and remains so. The radial gradient remains high and is not significantly affected. This suggests that, for all reasonable gas flow rates, the limiting radial thermal resistance is in the pipe wall and not at the interface between the inside wall and the gas.

Figures 14 to 18 show the variation of maximum temperature, maximum radial gradient, maximum circumferential gradient and maximum axial gradient as a function of gas speed with adjacent pipe diameter as a parameter. These results reflect a spacing of 25 feet. Similar trends are generated for each of the adjacent pipeline spacings listed in Table 2, which range from 10 to 50 feet.

The computational model indicates that:

- Gradients in the radial direction are of the order of $10^2$ to $10^3$ °C/m,
- Gradients in the circumferential direction are of the order of $10^1$ to $10^2$ °C/m, and
- Gradients in the axial direction are of the order of $10^0$ to $10^1$ °C/m

The ranges of these results imply that radial thermal stresses and circumferential stresses may be causes for concern. They show a strong effect of gas speed, which reflects the role of the flowing gas in transporting heat away from the impinged pipeline. Speeds in excess of 10 mph appear sufficient to cool the impinged area, whereas at speeds less than 5 mph there is the potential for significant local heating.

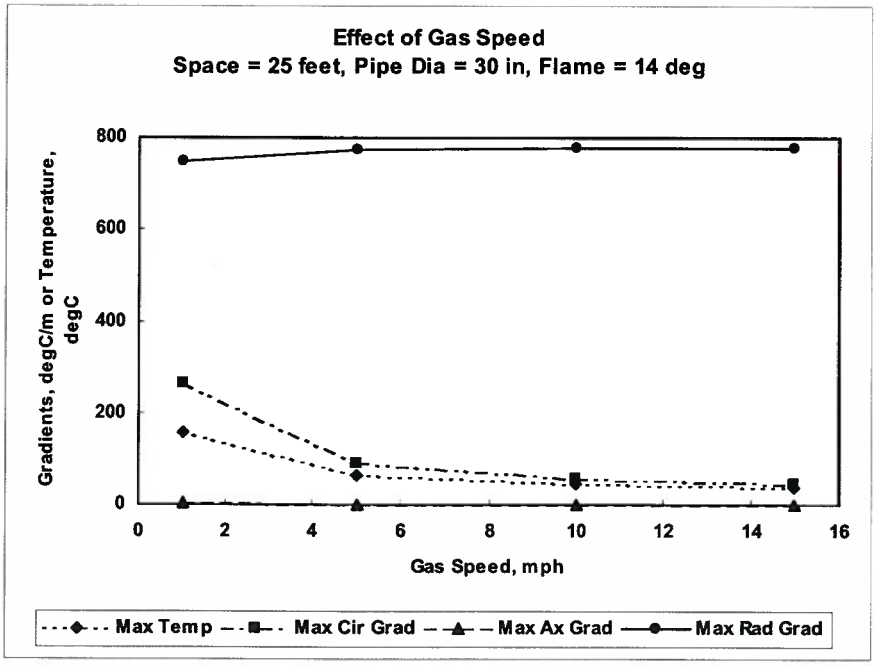


**Figure 14 Computed maximum temperature and temperature gradients in adjacent pipe as a function of gas speed**

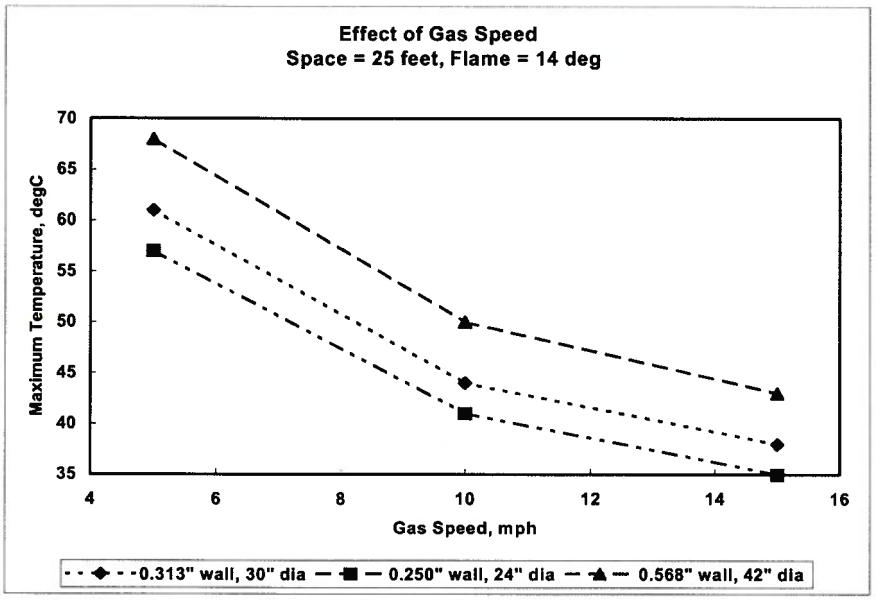


**Figure 15 Variation of computed maximum temperature with gas speed with adjacent pipe diameter as parameter**

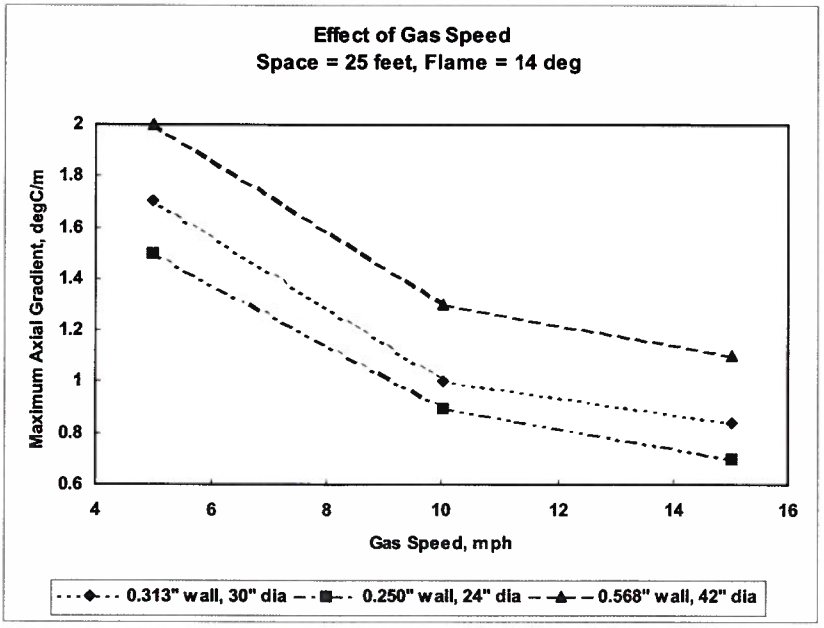


**Figure 16 Variation of computed maximum axial temperature gradient with gas speed with adjacent pipe diameter as parameter**

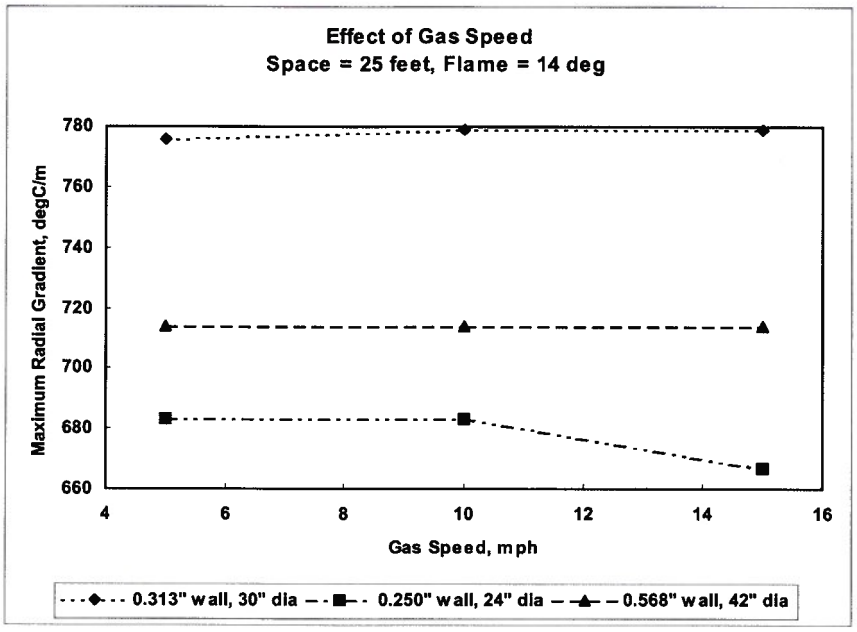


**Figure 17 Variation of computed maximum radial temperature gradient with gas speed with adjacent pipe diameter as parameter**

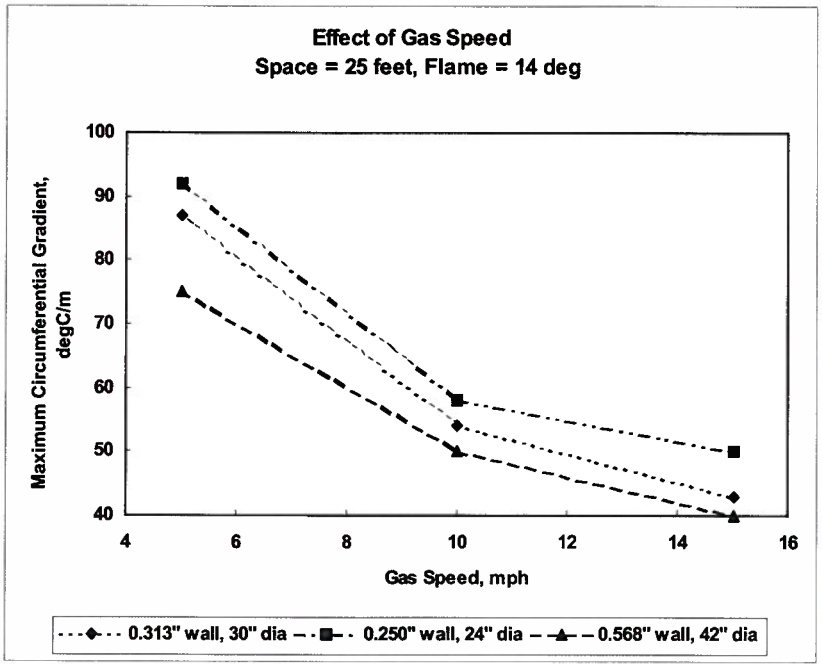


**Figure 18 Variation of computed maximum circumferential temperature gradient with gas speed with adjacent pipe diameter as parameter**

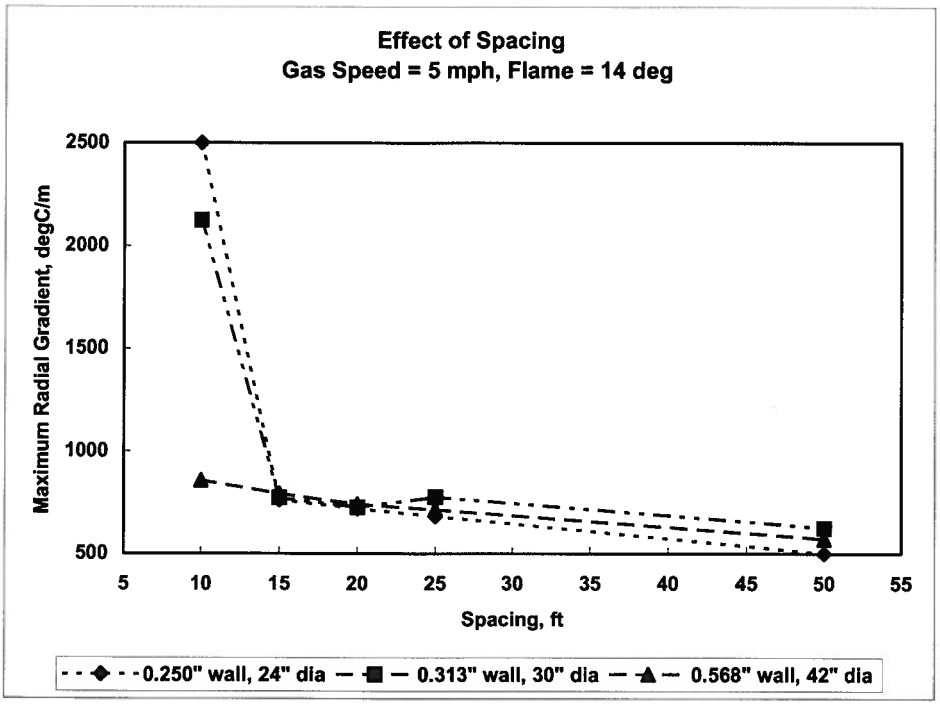


**Figure 19 Computed maximum radial temperature gradient as a function of spacing with diameter as a parameter**

Figure 19 shows the computed variation of the maximum radial gradient as a function pipe spacing. As the spacing increases, and the pipe diameter and wall thickness increase, the gradients become rapidly more benign and asymptote to a smaller value within computational convergence limits. For the fairly conservative conditions shown in Figure 19, spacings greater than 15 feet are essentially equivalent. Graphs like Figure 19 can be used as a basis for designating adequate adjacent pipeline spacings after the structural consequences of the thermal gradients are known. When such results are considered in light of the significant potential for local heating evident in Figure 14 at lower gas speeds, a spacing of 25 feet appears appropriate to avoid triggering an incident due to rupture on an adjacent gas-transmission pipeline.

## Discussion

Soil characterization in crater models is the greatest shortcoming. The fluid mechanics of pressurized gas escaping from an opening is reasonably well understood even if computation of the exact consequences are complicated by practical issues such as location of break, degree of subsequent misalignment of the pipes and so on. However, the soil response to the escaping gas jet is difficult to quantify based on available soil data. This may be attributed to the fact that the historical development of soil testing has been driven by civil engineering needs such as the construction of bridges and roads. Such designs seek properties of soils on a time scale and under loads that are significantly different from those encountered in pipeline leaks or ruptures. Therefore, it seems reasonable that specific soil tests need to be developed that can be used in analyzing the crater formation as a function of side-slit or guillotine rupture. These tests not only need to simulate the expected loads, but also need to be simple and need to represent soils on the length-scale of pipe excavation with one integrated measure.

The Gasunie-Delft models predict crater dimensions using empirical relations that are dependent on the depth of cover, pipe diameter, and soil type. It is noteworthy that these relationships do not contain gas pressure — i.e., the driving force. Therefore, the currently calculated crater depth scales with pipe diameter, with soil moisture or soil type as a parameter. If the crater width data are plotted against depth of burial, as shown as discrete points in Figure 20, a trend (indicated by the linear regression line) is evident except for two outliers.

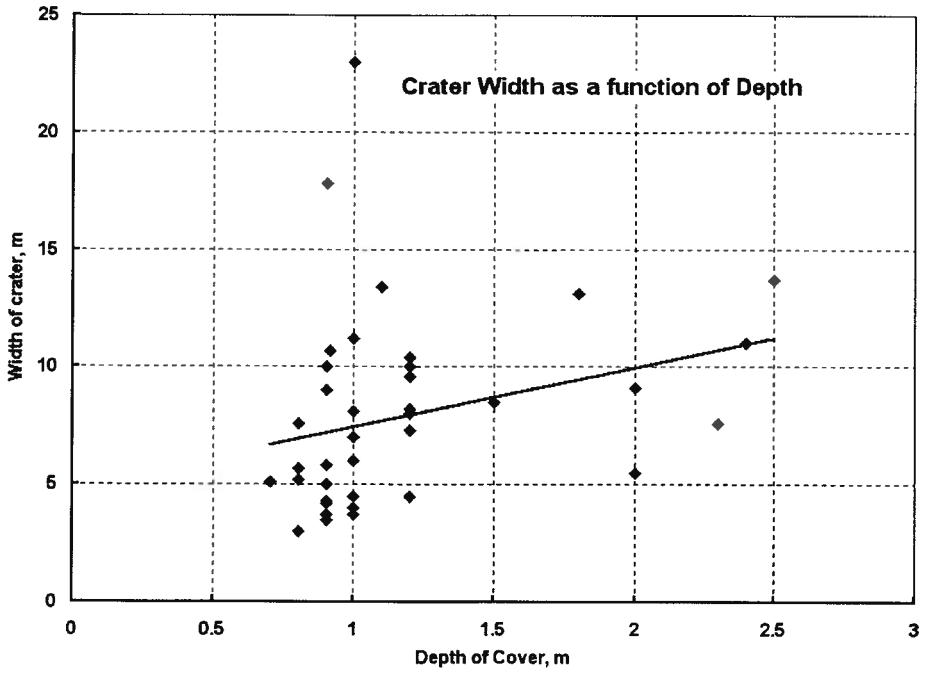


**Figure 20 Measured crater width vs depth of cover with linear regression line**

From ordnance theory, the crater width scales with crater depth, with no explicit appearance of gas pressure. It can be argued that the predicted crater depth should contain the gas pressure, and hence the crater dimensions would then rationally depend on the internal pressure of the ruptured pipe. This argument can be augmented by the hypothesis that for pressures greater than a threshold value, the crater width may be relatively insensitive to pressure because once pressure gains access to the atmospheric sink, no additional soil is displaced.

The calculations indicate that radiative effects diminish rapidly with distance. This is a result of the rapid decrease of the angle factor. Based on the results generated, a spacing of 25 feet appears adequate as long as gas flowing in adjacent line. It is critical that the gas in the adjacent line continues to flow, acting to transport away the heat absorbed by the pipe, thereby cooling the pipeline and avoiding creep-induced rupture. If the flow stops, a breach in the integrity of the adjacent line may occur. In the radiative analysis undertaken here, wind effects were not considered. The foregoing conclusion on spacing may need to be modified if a sustained wind causes flame to change significantly from the assumed conical shape.

Considerations other than triggering adjacent pipeline failure are also important in determining pipeline spacing. While not the subject of this work, it is appropriate to note that the practical considerations in pipeline construction and risks in contacting adjacent pipelines during rehabilitation lead to recommended right-of-way widths from 30 feet to more than 100 feet depending on locale, the diameter of the pipeline, and other circumstances. Such widths in the case of the larger-diameter pipelines are much larger than the minimum spacing to avoid triggering an adjacent pipeline failure, and so will continue to promote multiple-use corridors. It follows that care must be taken to separate strategic services and other pipelines from gas-transmission pipelines by on the order of 25 feet to ensure their survival in the event of an adjacent gas-transmission pipeline rupture.

# Conclusions

When a high-pressure pipeline experiences loss of integrity, there is an immediate risk to an adjacent pipeline if:

- the adjacent line was uncovered by the crater formed by the initial loss of integrity,
- the escaping gas ignites, and
- the wall temperature of the adjacent lines increases unacceptably because of radiative heating.

This sequence was modeled by using semi-empirical crater models and a numerical thermal model.

The conclusions are as follows:

- Pipeline spacings greater than 25 feet appear to be reasonable in reducing the potential for damage of adjacent pipelines.
- The effect of radiative flame heating diminishes rapidly as distance from the flame increases.
- Continuing gas flow in the adjacent pipeline greatly reduces the chance of damage.
- The soil response to the escaping gas needs to be better understood to obtain improved crater models. It may be that soil tests specifically designed to measure response to fluid impact are needed rather than classical civil engineering tests.

## References


1. "Ontgronding Door Gasleidingbreuk Verslag Modelonderzoek Berekeningen", Waterloop Kundig Laboratorium, Delft, M1136-R743.

2. "Herinterpretatie M1126", Waterloop Kundig Laboratorium, Delft, June 1991.

3. Mastbergen, D. R., "Ontgronding bij Persleidingbreuk: Herinterpretatie M1007", Waterloop Kundig Laboratorium, Delft, November 1991.

4. Schram, W., "Prediction of the Crater Caused by an Underground Pipeline Rupture", N. V. Nederlandse Gasunie, Report TR/T 97.R.2515, May 1997.

5. NEN 3651, Annex A: "Determining Disturbance Zone Dimensions", pp. 60-65.

6. Bagnold, R. A., "An Approach to the Sediment Transport Problem from General Physics", U.S. Geological Survey, Prof. Paper 422-I

7. Henrych, J., The Dynamics of Explosion and Its Use, Elsevier Scientific Publishing Company, 1979.

8. Croce, P. A., and Mudan, K. S., "Calculating Impacts for Large Open Hydrocarbon Fires," *Fire Safety Journal*, Volume 11, pp. 99-112, 1986.

9. Mudan, K. S., "Geometric View Factors for Thermal Radiation Hazard Assessment", *Fire Safety Journal*, Volume 12, pp. 89-96, 1987.

10. Anon., "Pipeline Route Selection Manual for Rural and Cross-Country Pipelines", Pipeline Division, American Society of Civil Engineers, Manual of Practice No. 46, 1995 (Draft).

11. Anon., "Temporary Right-of-Way Width Requirements for Pipeline Construction", final report to INGAA, from Gulf Interstate Engineering, 1999.

## Appendix A – Listing of Mathcad Sheet for Crater Model

# PRCI - Battelle/Gasunie Crater Model

**Enter**

**1) pipe diameter in meters, $D_p$**
**2) the depth of cover from ground surface to the top of the pipe, $D_c$ and**
**3) a value for the moisture content parameter, w, within the following framework**

**0.75 is very dry sand**
**1.1 is dry mixed soil or sand**
**1.75 is mixed soil or gravel**
**2.7 is humid mixed soil, clay or rock**
**5.0 means heavy clay**

**4) soil density in $kg/m^3$**
**5) gas specific heat ratio (1.301 for methane)**
**6) pressure of gas in pipe, $p_0$, in Pa**

**Outputs:**

**1) Crater depth, D**
**2) Crater width, W**

**Other nomenclature:**

**$u_x$ is the velocity of the explosive gases**
**ww is the distance from the ground to the center of the pipe**
**$R_p$ is the radius of the pipe**

Inputs: Test case

$\gamma := 1.301$

$w := 5$

$\rho_{soil} := 2050 \cdot \frac{kg}{m^3}$

$D_p := 1.067 \cdot m$

$D_c := 1.0 \cdot m$

$p_0 := 84.23 \cdot 10^5 \cdot Pa$

$R_p := \frac{D_p}{2}$

$ww := D_c + R_p$

Gasunie depth of crater formulation

$R(w) := 0.28 + 0.62 \cdot (5 - w) - 0.07 \cdot (25 - w^2)$

$R(w) = 0.28$

**Check that R is between 0.28 and 1.3**

$D := if\left(w \le 0.6, 4.3 \cdot D_p + D_c, 0\right)$

$D := if\left[(w - 0.6) \cdot (2 - w), \frac{R(w)}{0.3} \cdot D_p + D_c, D\right]$

$$D := \text{if}\left(2 \le w, 2.2 \cdot D_p + D_c, D\right)$$

$$D = 3.347\ \text{m}$$

**Check that D is reasonable**

$$u_x := \sqrt{\frac{\gamma \cdot p_0}{3 \cdot \rho_{soil} \cdot (\gamma^2 - 1)}}$$

$$u_x = 50.722\ \frac{\text{m}}{\text{s}}$$

$$u_{kr} := 2.54 \cdot \frac{\text{m}}{\text{s}}$$

This value of ukr was obtained empirically from non-Gasunie data

$$W := 2 \cdot \sqrt{\frac{D_p \cdot ww}{u_{kr}} \cdot \sqrt{\frac{\gamma \cdot p_0}{3 \cdot \rho_{soil} \cdot (\gamma^2 - 1)}} - ww^2}$$

$$W = 11.013\ \text{m}$$